



**HAL**  
open science

# CFD Analysis of a Steam Generator Separation Test in the Kozloduy VVER-1000 Reactor

Q. Feng, U. Bieder

► **To cite this version:**

Q. Feng, U. Bieder. CFD Analysis of a Steam Generator Separation Test in the Kozloduy VVER-1000 Reactor. NUTHOS-11 The 11th International Topical Meeting on Nuclear Reactor Thermal Hydraulics, Operation and Safety, Oct 2016, Gyeongju, South Korea. cea-02438706

**HAL Id: cea-02438706**

**<https://cea.hal.science/cea-02438706>**

Submitted on 27 Feb 2020

**HAL** is a multi-disciplinary open access archive for the deposit and dissemination of scientific research documents, whether they are published or not. The documents may come from teaching and research institutions in France or abroad, or from public or private research centers.

L'archive ouverte pluridisciplinaire **HAL**, est destinée au dépôt et à la diffusion de documents scientifiques de niveau recherche, publiés ou non, émanant des établissements d'enseignement et de recherche français ou étrangers, des laboratoires publics ou privés.

## CFD Analysis of a Steam Generator Separation Test in the Kozloduy VVER-1000 Reactor

Feng Q., Bieder U.\*

DEN-STMF, CEA, Université Paris-Saclay  
F-91191 Gif-sur-Yvette; France  
Ulrich.BIEDER@cea.fr

### ABSTRACT

Computational fluid dynamics (CFD) research for nuclear reactor safety dedicates to real scale reactor circuits under realistic thermal hydraulic conditions. In the framework of an OECD/NEA benchmark, CEA has attempted 10 years ago with the code TrioCFD to study the temperature distribution at the core inlet in a main steam line break (MSLB) accident scenario in a Bulgarian VVER1000 reactor. This work is resumed here by completing the geometry of the reactor pressure vessel (RPV) and by capitalizing both code development and high performance computing (HPC) resources.

Before modelling the full scale RPV thermal-hydraulics, a PIRT (Phenomena Identification and Ranking Table) was performed to classify the existing physical phenomena in a ranking table. Three single effect validation test cases were defined in a test matrix. The CFD approach was validated *single effect by single effect* by reproducing the defined well suited test cases.

The core outlet temperature distribution was measured during a commissioning steam generator separation test at Kozloduy nuclear power plant. This temperature distribution is compared to the CFD calculations and helps to validate *integrally* the full scale reactor calculation. Tetrahedral meshes of 50 to 400 million velocity control volumes were generated for the complete RPV; self-evidently the mesh refinement reflects the restrictions of the former defined test matrix.

In the OECD benchmark, the core inlet temperature was calculated from the measured core outlet temperature by simple energy conservation. With the integral calculation we were able to review this process with the calculated core inlet and outlet temperature.

### KEYWORDS

VVER-1000, MSLB, CFD, VALIDATION, HPC

### 1. INTRODUCTION

The mixing of loop flows in the reactor vessel of VVER-1000 V320 were presented in Exercise 1 of VVER-1000 Coolant Transient Benchmarks (V1000CT) by OECD/NEA [1, 2]. Starting from nearly symmetric hydraulic states, thermal asymmetric loop operation in different combinations was caused by disturbing the steam flow of one or more steam generators (SG). During the tests all main coolant pumps were in operation. Both loop heat-up and loop cool-down were considered in the experiments. For the heat-up tests the pressure in the steam generator was first increased by closing the steam isolation valve (SIV) and isolating the SG from feed water. Then the pressure was stabilized by steam dump to the atmosphere.

Non-uniform and asymmetric loop flow mixing in the reactor vessel has been observed in the event of such thermal asymmetric loop operation. Such asymmetric flow distribution was reproduced and analyzed with Trio\_U code using CAD data of the fabricated reactor pressure vessel [3]. However, the reactor part above the core inlet was not modelled and the perforated core barrel and support columns were modelled by flow resistance. In order to complete the reactor model, a porous model and volumetric heat sources are introduced in the core region and the upper plenum with the hot legs were

added by Boettcher [4]. However, perforated part of support columns in the lower plenum was modelled by additional flow resistance. The construction internals have a strong influence on the flow field and on the mixing. Therefore the inlet region, the downcomer below the inlet region, the eight spacer elements in the downcomer and the lower plenum structures (the perforated elliptical sieve plate) are represented more accurately [5]. However, this study assumed that the PWR consisted only of 64 fuel rods and only the shell side of the reactor was modelled.

The subject of this work is using TrioCFD code to calculate the mixing coefficients, temperature and pressure distribution with a complete reactor model which includes all geometrical details such as the cold- and hot leg inlet nozzles, the downcomer, the lower and upper plenum. Only the core region is treated as porous media.

## 2. SPECIFIC FEATURES OF VVER-1000

VVER-1000 is a four-loop pressurized water reactor with hexagonal assembly geometry and horizontal steam generators. The steam is supplied to a 1000 MWe turbine. The core is of open type and contains about 163 hexagonal fuel assemblies. The fuel pins are arranged in a triangular grid. Most of the reactor internals are contained in the core barrel, which is inserted and fixed in the reactor vessel. The primary circuit coolant flows to the core through the perforated barrel bottom (1344 holes) (Fig.1) passes into the fuel support columns which are serving as flow distributors. In fact, the upper part of the hollow support columns are inserted into corresponding holes of the core support plate and welded together at the top so that all the flow passes through the support columns. In this way, the primary coolant flows through the slots into the support columns and then further upward through the support plate into the fuel assemblies. At the upper core plate, most of the fuel assembly heads are connected to shielding tubes, located in the upper plenum, to protect the control rods and instrumentation cables from mechanical impacts.

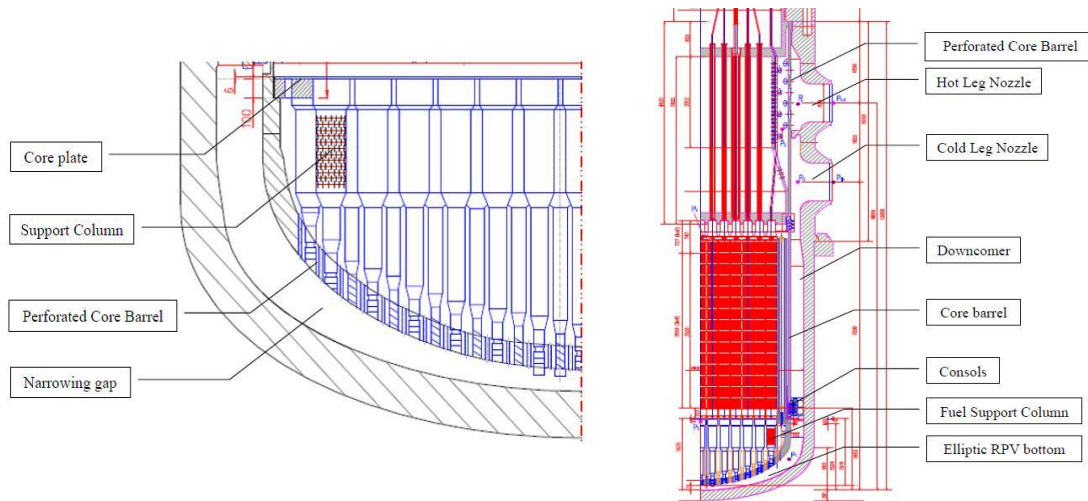


Fig. 1: Main components within a VVER-1000 lower plenum (left) and reactor pressure vessel (right)

## 3. THE VVER-1000 MIXING EXPERIMENTS

The mixing experiment was initiated by isolating the steam generator of loop 1 (SG-1). Three states were considered: initial, transient and final stabilized state. These states are described below. After the stabilization of the pressure and the core outlet temperature, the experiment was repeated for loop 2. The transient caused by disturbing loop 1 is selected for the coolant mixing analysis and the data of the second experiment was used indirectly by OECD/NEA to support the analysis [1, 2].

### 3.1. Initial State

All four main coolant pumps and four steam generators are in operation. The thermal power of 281MW was about 9.36 % of the nominal power. With 15.59 MPa, the pressure above the core was close to the nominal value of 15.7 MPa. The coolant temperature at the reactor inlet was 268.6 °C, about 20 °C lower than the nominal value. The boron acid concentration was 7.2 g/kg, close to the value of 7.5 g/kg at which the coolant temperature reactivity coefficient is zero.

For this initial state, the relative fuel assembly temperature rise of each assembly with temperature control was calculated by Kolev et al [1-2] from 95 measured cold leg and assembly outlet temperatures. The temperature distribution at the core outlet in the initial state is shown on the left of Fig. 2 for the 95 of totally 163 fuel assemblies. The measured temperature rise is used to approximately distribute the core power among fuel assemblies. For assemblies without temperature control, the temperature rise in the initial state is estimated using the core symmetry at beginning of life. The average heat-up over the core was used to normalize the temperature rise distribution, which leads to an average fuel assembly heat-up of 3.2°C.

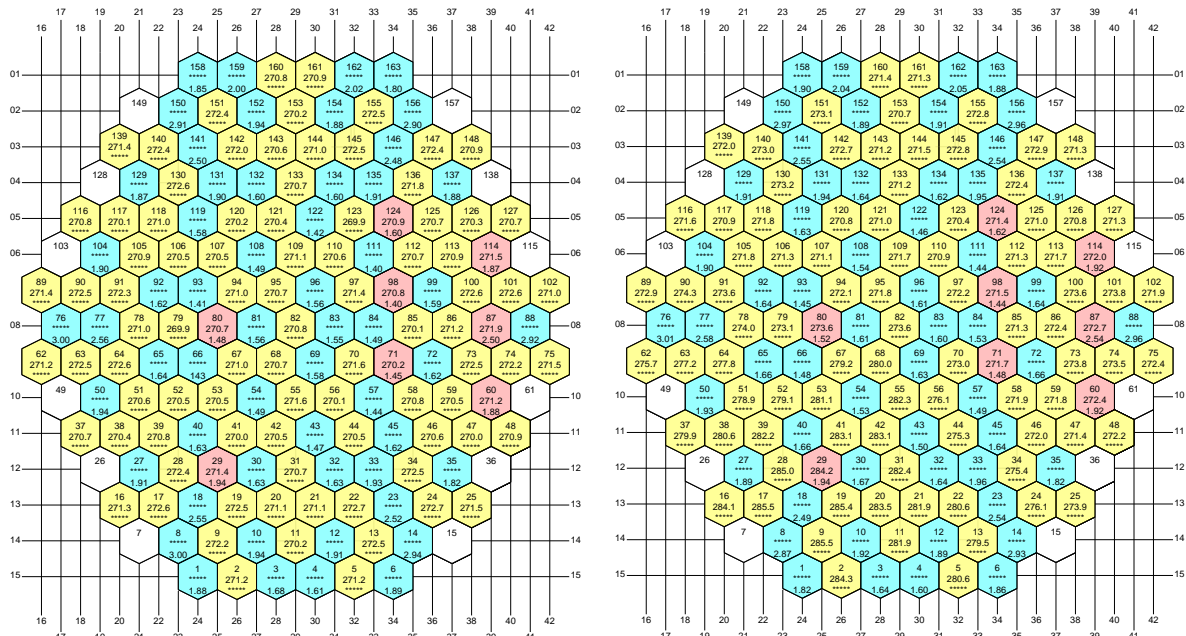


Fig. 2: Distribution of core outlet temperature in the initial (left) and final state (right) [1]

### 3.2. Transient

A transient was initiated by closing the steam isolation valve of SG-1 for isolating SG-1 from feed water. The pressure in the secondary side of SG-1 started to increase and stabilized in about 20 min to 6.47 MPa. The pressure maintained approximately constant during the transient by operating the steam dump to condenser. The coolant temperature in loop 1 raised by 13.6°C and the mass flow rate decreased by about 3.6%. The temperature in the other loops increased slightly due to the mixing of loop flows. The mass flow through the reactor decreased by 1%. After about 90s transient time, the temperature of cold leg 1 exceeded that of the hot leg; the difference stabilized to 0.6-0.8°C in about 25 minutes. During the transient, the core power changes only by 0.16% and the initially constant and symmetric core power distribution does not change significantly.

### 3.3 Final State

The stabilized state at 1800s from the onset of the transient is considered as “final state”. The measured core outlet temperature distribution is shown on the right of Fig.2. For the assembly number  $i$ , the inlet temperatures  $T_{in,i}$  in the final state were obtained by Kolev et al [1-2] from the corresponding measured outlet temperature  $T_{out,i}$  and the estimated fuel assembly temperature rise in the initial state  $\Delta T_i$ . The local temperature rise during the transient is assumed to be the same as in the initial state as a consequence of the constant normalized core power distribution:

$$T_{in,i} = T_{out,i} - \Delta T_i \quad i = 1 \dots 163 \quad .$$

## 4. THE TrioCFD CODE

TrioCFD (previously named “Trio\_U”) is a Computational Fluid Dynamics (CFD) code based on the TRUST platform [13]. The code is developed at CEA-Saclay and has been especially designed for incompressible, turbulent flows in complex geometries. The platform independent code is based on an object oriented, intrinsically parallel approach and is coded in C++. The flexible code structure allows the user to choose a suitable discretization method and to combine various appropriate physical models. Several convection and time marching schemes as well as wide range of boundary conditions are available [11-12].

### 4.1. Conservation Equations

In Reynolds-averaged approaches to turbulence, the non-linearity of the Navier-Stokes equations gives rise to Reynolds stress terms that are modeled by turbulence models. Almost all turbulence models for industrial applications are based on the concept of eddy-viscosity for the Reynolds stress. This approach leads in matrix notation to:

$$-\overline{u_i' u_j'} = \nu_T \cdot \left( \frac{\partial U_i}{\partial x_j} + \frac{\partial U_j}{\partial x_i} \right) - \frac{2}{3} k \delta_{ij} \quad (2)$$

The following Reynolds averaged mass conservation equation, Navier-Stokes equations (RANS) and energy conservation equation are solved for incompressible flows:

$$\frac{\partial U_i}{\partial x_i} = 0 \quad , \quad (3)$$

$$\frac{\partial U_i}{\partial t} + \frac{\partial U_i U_j}{\partial x_j} = -\frac{\partial P}{\partial x_i} + \frac{\partial}{\partial x_j} \left[ (\nu + \nu_T) \cdot \left( \frac{\partial U_i}{\partial x_j} + \frac{\partial U_j}{\partial x_i} \right) \right] + S_{m,i} \quad , \quad (4)$$

$$\frac{\partial T}{\partial t} + \frac{\partial U_j T}{\partial x_j} = \frac{\partial}{\partial x_j} \left( (a + a_t) \frac{\partial T}{\partial x_j} \right) + S_{th} \quad . \quad (5)$$

Here  $S_{m,i}$  represents a momentum source term and  $S_{th}$  is an energy source term.

### 4.2 Turbulence Modelling: the k-ε model

In the study presented here, the turbulent viscosity is calculated from the well-known k-ε model by using the following isothermal formulation:

$$\nu_t = C_\mu \frac{k^2}{\varepsilon} \quad (6)$$

$$\frac{\partial k}{\partial t} + \frac{\partial(U_j k)}{\partial x_j} = \frac{\partial}{\partial x_j} \left[ \left( \nu + \frac{\nu_t}{\sigma_k} \right) \frac{\partial k}{\partial x_j} \right] - \varepsilon + P \quad (7)$$

$$\frac{\partial \varepsilon}{\partial t} + \frac{\partial(U_j \varepsilon)}{\partial x_j} = \frac{\partial}{\partial x_j} \left[ \left( \nu + \frac{\nu_t}{\sigma_\varepsilon} \right) \frac{\partial \varepsilon}{\partial x_j} \right] + C_{\varepsilon 1} P \frac{\varepsilon}{k} - C_{\varepsilon 2} \frac{\varepsilon^2}{k} \quad (8)$$

$$P = -\overline{u_i' u_j'} \frac{\partial U_i}{\partial x_j}, \quad \text{with } \overline{u_i' u_j'} \text{ calculated by eq.(2)} \quad (9)$$

The following empirical coefficients are used:  $C_\mu=0.09$ ,  $\sigma_k=1$ ,  $\sigma_\varepsilon=1.3$ ,  $C_{\varepsilon 1}=1.44$ ,  $C_{\varepsilon 2}=1.92$ . The presence of anisotropic turbulence represents the weak point of linear eddy-viscosity models, and in particular of the k- $\varepsilon$  model. Hence, such models may provide incorrect results in non-trivial cases, such as the in presence of wall curvature, impinging jets or boundary layer detachment and re-attachment.

#### 4.4. Discretization

In TrioCFD, the conservation equations can be discretized on unstructured, tetrahedral grids by using a finite volume based finite element method (Finite Volume Elements, VEF). The discretization is an extension of the classical Crouzeix–Raviart element where the main vector unknowns (velocity) and scalar unknowns (temperature,  $k$ ,  $\varepsilon$  and concentration) are located in the center of the faces of an element whereas the pressure is discretized in both the center and the vertices of the element. This staggered mesh arrangement is P1-non-conforming for velocity and scalars and P0-P1 for the pressure.

#### 4.5. Solution Method

After discretization, a system of non-linear algebraic equations is obtained whose unknowns are the discrete physical variables. Explicit and implicit time marching schemes are available in TrioCFD. Here the Implicit Euler backward time scheme is used to integrate the conservation equations in time, hence only the implicit scheme is presented. Temporal integration of Navier-Stokes equations is done in two steps (“fractional steps” method) [7]:

1. A Reynolds averaged non-divergence free velocity field  $U^*$  is calculated with the linear system solver GMRES. The convection term is linearized. In vector notation this leads for eq.(4) to:

$$\frac{U^* - U^n}{\Delta t} = -\nabla P^n - \nabla \cdot [(\nu + \nu_t) \cdot (\nabla U^* + \nabla^T U^*)] - \nabla \cdot (U^n U^*) + S_m \quad (10)$$

2. The velocity field  $U^*$  is then projected with the conjugated gradient method of the pressure solver into a divergence free space [6]:

$$\Delta \delta P = \nabla \cdot U^*, \quad P^{n+1} = P^n + \delta P, \quad U^{n+1} = U^* - \frac{\nabla \delta P}{\Delta t} \quad (11)$$

### 5. PIRT ANALYSIS

To ensure the capability of the CFD tools to simulate the application and assess the value of a quantity of interest with pre-defined accuracy, PIRT (Phenomena Identification and Ranking Table) analysis is a fundamental step that identifies the key phenomena involved in the industrial application. More details about PIRT are available in [9-10]. Firstly, the pressure drop is selected as the figure of merit and the aimed precision is defined to below 10% difference to experimental values. The Reynolds number is assumed to determine the predominant flow physics. Three separate effect validation tests are defined which present predominant physical phenomena in the VVER-1000 steam generator separation test. These tests are given in Table 1 and discussed in the following chapters.

Table 1. Separate effect tests

Location in the reactor	Physical phenomena	Re	Separate effect test
Downcomer	Boundary layer flow	3.1E+7	Turbulent channel
Perforated plates	Flow through holes	4.5E+6	Orifice flow
Cold leg nozzle	Impinging confined jet	7.0E+7	Baffle impact flow

### 5.1. Separate effect test “turbulent channel flow”

As the diameter of the reactor vessel (4 m) is much bigger than the thickness of the downcomer (0.25 m), flow in the downcomer can be simulated in first approximation as flow in a channel (Fig.3) with the same hydraulic diameter. The pressure gradient reference value of 0.370 kPa/m was calculated from correlations given by Idelchik [11] for the Re number given in Table 1.

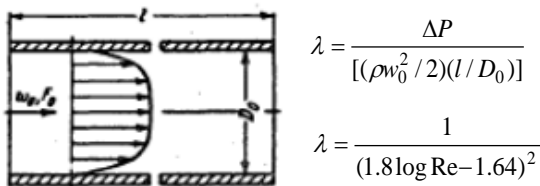


Fig. 3: Mean axial velocity profile and correlation

Table 2. Estimated pressure gradient

mesh size	y <sup>+</sup> 1 <sup>st</sup> point	Pressure gradient	Difference
7 mm	3772	0.336 kPa/m	7.69 %
3 mm	1563	0.320 kPa/m	12.08 %
1 mm	509	0.368 kPa/m	1.09 %

The calculated mean axial pressure gradient in the channel is compared in Table 2 to the reference value of the correlation. A y<sup>+</sup> value of about 1000 is thus aimed for the downcomer mesh of the reactor calculation.

### 5.2. Separate effect test “orifice flow”

In the VVER-1000 lower plenum, coolant passes at high velocity through the elliptic plate with 1344 holes given in Fig. 4. A 1 and 4 orifice model was built and mesh sensitivity is tested with five refinements of the meshing in the orifices. The pressure loss reference value 80.8 kPa for 1 orifice and 91.2 kPa for 4 orifices were calculated from a correlation given by Idelchik [11] for the Re number given in Table 1. The correlation is added to Table 3.

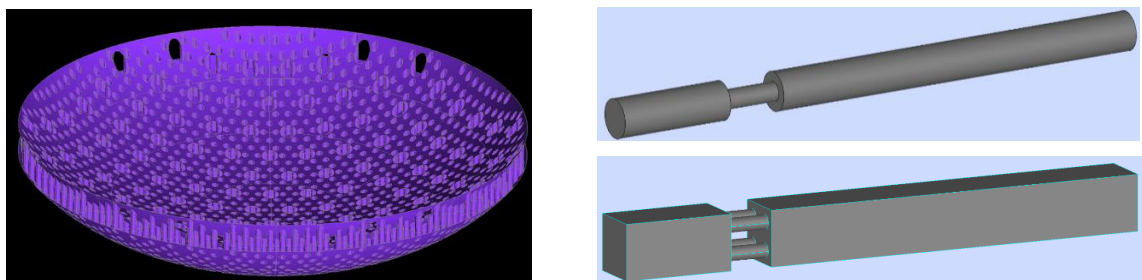


Fig. 4: CAD models of perforated core barrel and separate effect tests

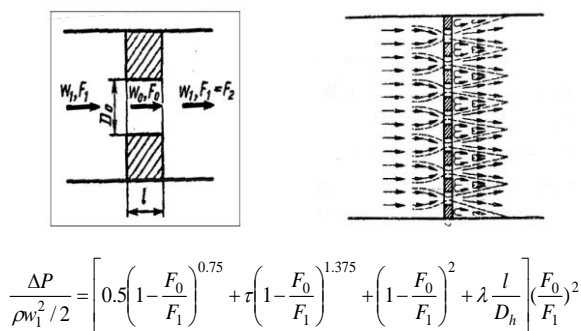


Fig. 5: Orifices and correlation

Table 3: Pressure loss of one and four orifice

Mesh size in orifice (mm)	Pressure loss one orifice (kPa)	Error (%)	Pressure loss four orifices (kPa)	Error (%)
8	135,2	67.3	—	—
6	114,5	41.7	—	—
5	103,4	27.9	—	—
4	89,43	10.6	101,1	10.9
3	83,95	3.9	96,56	5.9

For the real scale VVER-1000 model, the mesh refinement which gives a relative error of about 10% is aimed for the discretization of the holes in perforated plates (core support and outlet plates) and barrels (elliptic barrel in the lower plenum and cylindrical barrels in the upper plenum).

### 5.3. Separate effect test “baffle impact flow”

Coolant entering the downcomer by the cold leg nozzle with a high velocity can be modelled by a discharge from a straight tube with rounded edges against a baffle. Fig. 6 shows a 1/6 model of the cold leg nozzle with the impinging jet. Symmetry boundary condition is imposed in azimuthal direction.

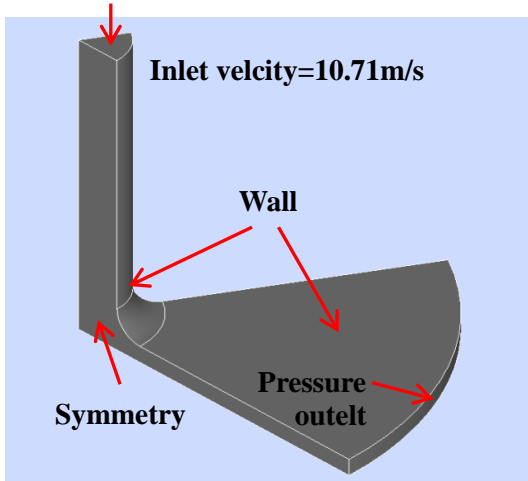


Fig. 6: CAD model of the cold leg nozzle separate effect test

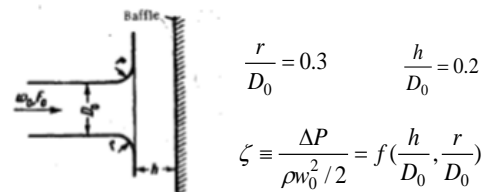


Fig. 7: Baffle description and pressure loss correlation

Table 4: Pressure loss dependent on mesh size

Mesh size (mm)	Pressure loss (kPa)	Error (%)
20	9.7	50.5
12	9.0	58.3
10	8.7	59.5

Using 3 refined meshes of 1 million to 6 million elements, the calculated pressure losses showed almost the same relative different to the reference value of 21.6 kPa (Table 4) taken from the correlation of Idelchik [11] given in Fig.7. Hence a mesh independent pressure loss value can be considered to be obtained, however the aimed accuracy could not have been achieved. The reason for the discrepancy is probably that the k-ε model is based on the hypothesis of fully developed, isotropic turbulent flow where the Reynolds stress tensor is aligned to the main strain rate tensor. This hypothesis is not correct for the cold leg jet impinging on the core barrel.

### 5.4 Validation and Application Domains

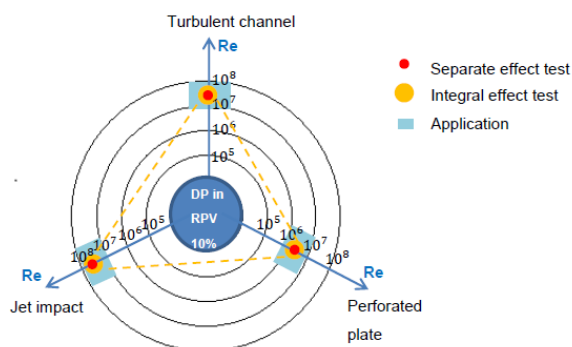


Fig. 8: Application and validation domain for the VVER-1000 Coolant Transient

Fig. 8 represents a sketch to visualize the overlap of the forthcoming application domain (mixing in the reactor pressure vessel at nominal thermal hydraulic conditions) with the integral and separate effect validation tests. The application domain appears as light blue colored areas. The presented separate effect tests appear as red dots; the integral test (the VVER-1000 steam generator separation test) appears as large yellow dots. These points are linked on the chart with dotted lines. It is visible that each dominant physical phenomenon of the forthcoming application is studied by a separate effect test and is covered by the integral test. Thus all the validation work is consistent with the application domain.

## 6. MODELLING OF THE KOZLODUY-6 MIXING EXPERIMENT

### 6.1. Meshing of the Flow Domain

In flow direction, the simulated domain starts about 15 m upstream of the RPV inlet nozzles and ends about 15 m downstream of the RPV outlet nozzles. A coarse tetrahedral mesh of about 50 million elements has been created using the commercial mesh generator ICEM. From the surface mesh extracted from a preliminary tetrahedral mesh created by the OCTREE method, a final mesh was created by the DELAUNY method; two prism layers were added. In order to create a fine mesh, this coarse mesh has been refined isotopically by using algorithm which cuts each tetrahedral element into 8 new ones; 400 million tetrahedral cells. Using the VEF discretization described in chapter 4.4, 100 million control volumes for each velocity component of the momentum equations were created for the coarse mesh and 800 million for the fine mesh. Fig. 9 shows the mesh refinement in the lower plenum. The fine mesh respects the mesh refinement defined in the separate effect test.

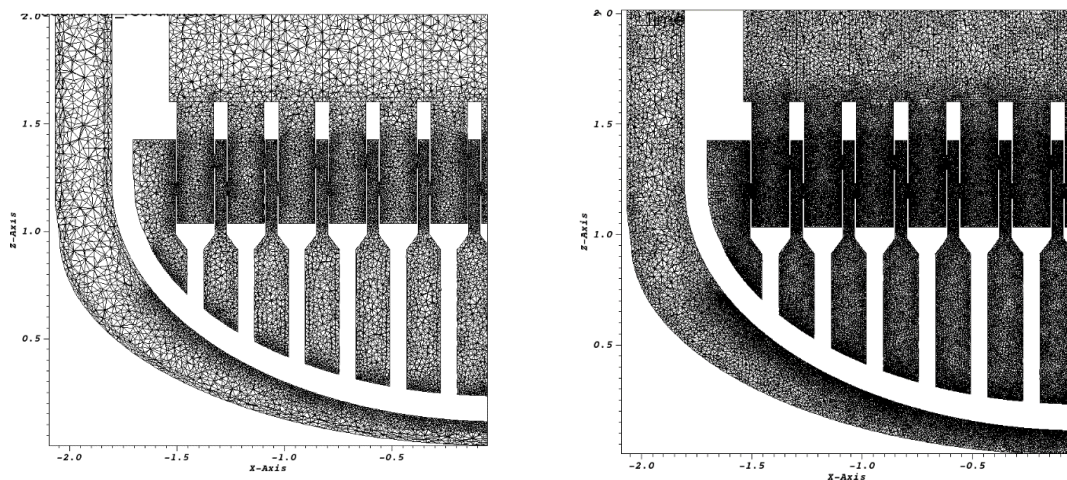


Fig. 9: Coarse mesh (left) and fine mesh (right) of the lower plenum of VVER-1000 reactor

### 6.2. Modelling of the core region

An explicit resolution of the reactor core is not possible to date. Thus, simplifications were introduced which lead to a basic porosity modeling of the core region. In the VVER-1000 core about 46% of the volume is blocked by fuel pins; hence a homogeneous volume porosity of 0.54 is introduced in the calculation. To take into account both the horizontal and vertical pressure losses in fuel assemblies, friction coefficients defined by correlation (eq.12) and Table 5 are used. This pressure loss is implemented in the Navier-Stokes equations (eq.4) as source term  $S_{m,i}$  [12].

Table 5. Parameters for the pressure loss correlation

Direction	$a$	$b$	$U$	$D$
Axial	0.316	0.25	$ \bar{u}_a $	$D_h$
Transverse	4.03	0.27	$ \bar{u}_t $	$D_e$

$$C_f = a \text{Re}^{-b} \quad \text{with} \quad \text{Re} = \frac{UD}{\nu} \quad (12)$$

### 6.3. Boundary Conditions

At the inflow faces of all the cold legs and the outflow faces of three hot legs, Dirichlet boundary conditions (imposed velocity and temperature) are used to simulate the flow in closed loops. The conditions after SG separation are detailed in Table 6. Fully developed turbulent flow is assumed to calculate inflow conditions in the cold loops for  $k$  and  $\epsilon$ . Von Neumann boundary condition (imposed pressure) is used to simulate a free outflow at the hot leg 4. Adiabatic walls and logarithmic wall functions are applied at all solid structures bounding the flow domain.

The fluid is assumed to be incompressible and the temperature dependency of the density is considered by the Boussinesq approximation. The physical properties of the fluid are those of pure water at 270°C and 16 MPa [3].

Table 6. Boundary conditions for the final state calculation

Loop	Velocity (m/s)		Temp. (°C)
	Cold leg	Hot leg	Cold leg
1	10.71069	10.71069	282.2
2	10.69599	10.69599	269.9
3	10.71069	10.71069	269.0
4	10.89181	P=0	269.2

## 7. SIMULATION OF THE MIXING EXPERIMENT

Flow and temperature field at the final state is assumed to be independent of both the initial state and the transient. Thus, an implicit solution scheme has been used with constant boundary conditions. A transient of about 7 to 9 s has been carried out until the temperature has reached steady state solution. Up to 40 hours on up to 10000 processor cores of the TGCC computer CURIE were necessary to converge the solution.

The Temperature distribution of the vessel wall is shown in Fig. 10. The flow does not rotate significantly in counter clockwise direction due to the non-uniform and asymmetric azimuthal distribution of the cold leg nozzle as detected experimentally and in the calculation of Bieder et al. [3].

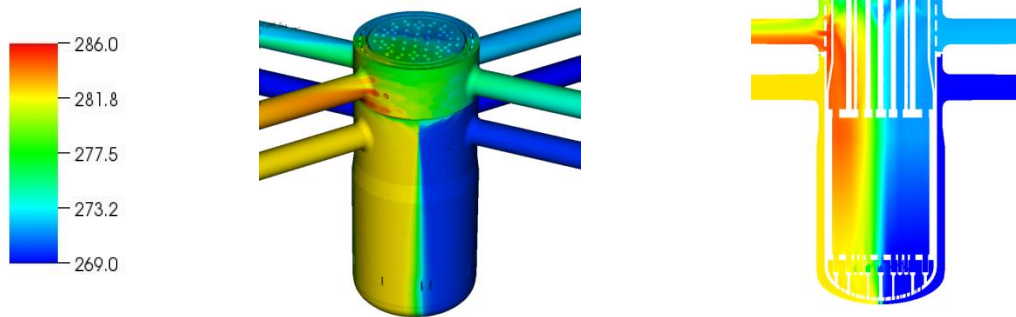


Fig. 10: Calculated temperature field in the RPV of the VVER-1000 reactor

### 7.1 Temperature distribution before steam generator separation

Comparison of the measured and calculated coolant temperature at the core outlet before closing the steam generator isolation valve SIV-1 is shown Fig. 11. As temperature was measured by only one thermocouple per assembly, the experimental temperature map is discontinuous. Missing values have been interpolated linearly. The calculated temperature map is continuous and in agreement to the measured map (slightly overestimated). Quantitative values are compared along the dotted line for the coarse (50M) and fine mesh (350M).

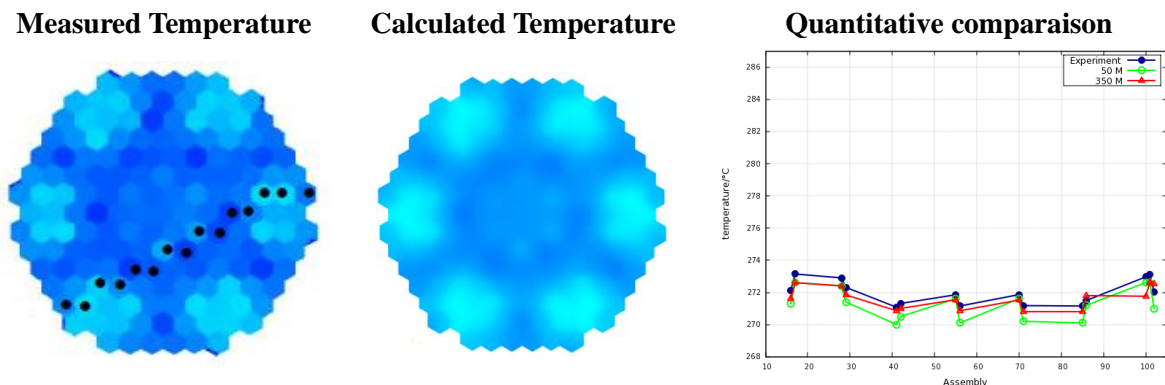


Fig. 11: Measured and calculated temperature at the core outlet before closing SIV-1

## 7.2 Temperature distribution after steam generator separation

### 7.2.1 Temperature distribution at the core inlet

Comparison of the measured and calculated coolant temperature at the core inlet after closing SIV-1 is shown in Fig. 12. It can be seen that measured flow center maximum of the flow coming from cold leg #1 is displaced in counter clockwise direction (by about 24° to be precise). The displacement calculated by the k-ε model shows a smaller angle and the maximum temperature is slightly overestimated as can be seen from the temperature profile along the dotted line.

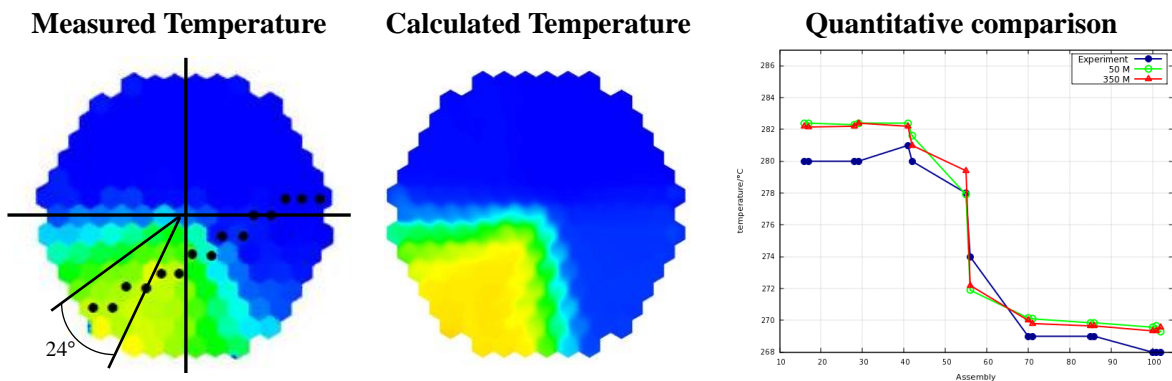


Fig. 12: Measured and calculated temperatures at the core inlet after closing SIV-1

### 7.2.2 Temperature distribution at the core outlet

Comparison of the measured and calculated coolant temperature at the core outlet after closing SIV-1 is shown in Fig. 13. It can be seen that the calculated hotter temperature from cold leg #1 covers a bigger area than in the core inlet plane (Fig.12) but is very close to the measured area. The calculation slightly overestimates the measurement; this can be seen from the quantitative comparison along the dotted line.

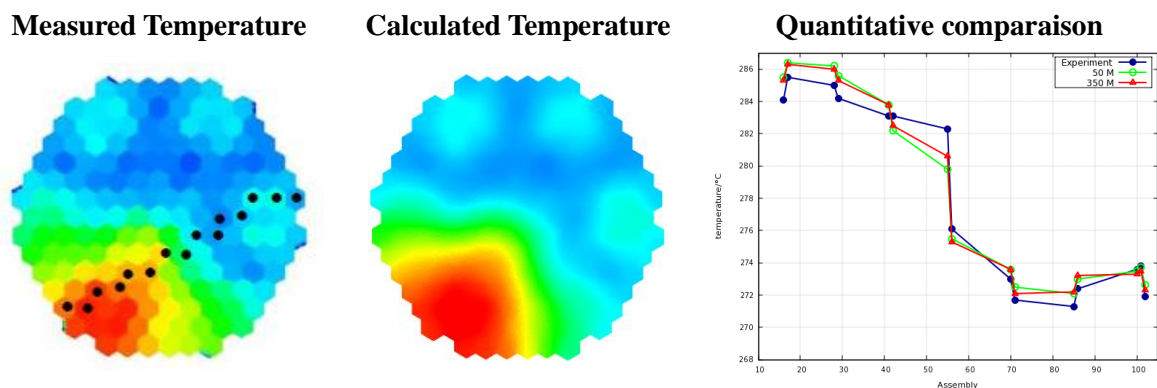


Fig. 13: Measured and calculated temperatures at the core outlet after closing SIV-1

It seems possible that the linear extrapolation of the experimental core outlet temperature to the core inlet underestimates the mixing in the core region and thus overestimates the affected area and underestimated maximum temperatures.

## 7.3. Loop to Fuel Assembly and Loop to Loop Mixing Coefficients

Loop to fuel assembly mixing coefficients  $K_{ij}$  are defined by as the ratio (in %) of coolant from loop  $i$  to the total flow through the assembly  $j$ . These mixing coefficients have been determined in the calculation by means of four different passive scalars, which are injected at each inlet nozzle with a concentration of 100%. The specific scalar  $i$  is transported from loop  $i$  to the core entry. The concentration of each specific scalar at the assembly inlet  $j$  refers to the mixing coefficient  $K_{ij}$ . All

mixing coefficients are collected in the mixing matrix of the whole core inlet. The measured and calculated loop to fuel assembly mixing coefficients are given in Fig. 14. An overestimation of mixing is detected in the calculation, however, this can also be related to the experimental calculation procedure.

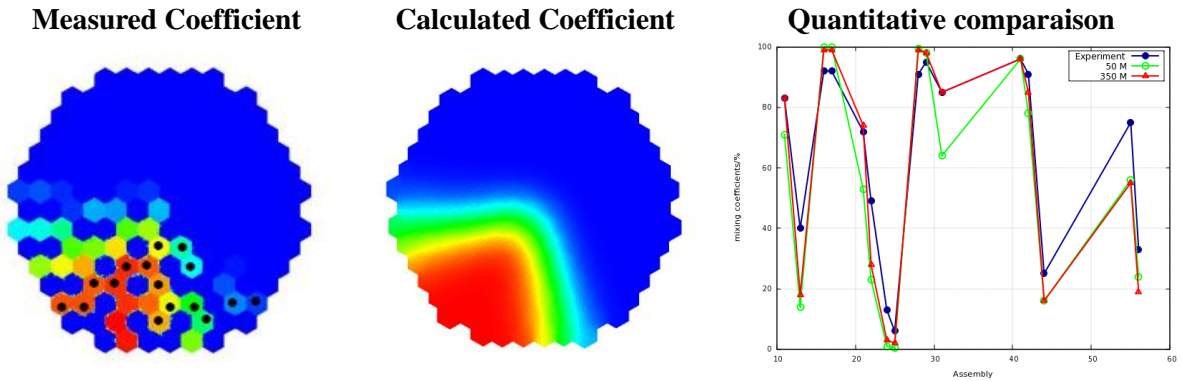


Fig. 14: Comparison of loop to fuel assembly mixing coefficients

The loop to loop mixing coefficients  $K_{ij}$  in the flow path from cold leg  $i$  to cold leg  $j$  are defined as the ratio of the coolant flow from loop  $i$  into loop  $j$  to the total flow in loop  $j$ . The measured and calculated mixing coefficients are shown in Table 7. It can be seen that the mixing coefficients are very accurately predicted by the calculation.

Table 7. Loop to loop mixing coefficients

$K_{ij}$	Experiment	Calculation
$K_{12}$	0.12	0.1183
$K_{21}$	0.10	0.09852
$K_{41}$	0.16	0.1572
$K_{32}$	0.14	0.1391

### 7.5. Velocity Distribution at the Core Inlet

The velocity distribution in vertical and horizontal cut planes is shown in Fig. 15. The acceleration of the flow in the cold leg nozzles and in the elliptic perforated core barrel is clearly visible. Higher velocities are also detected in the periphery of the core support plate, which was as well observed in the Kozloduy-5 experiment.

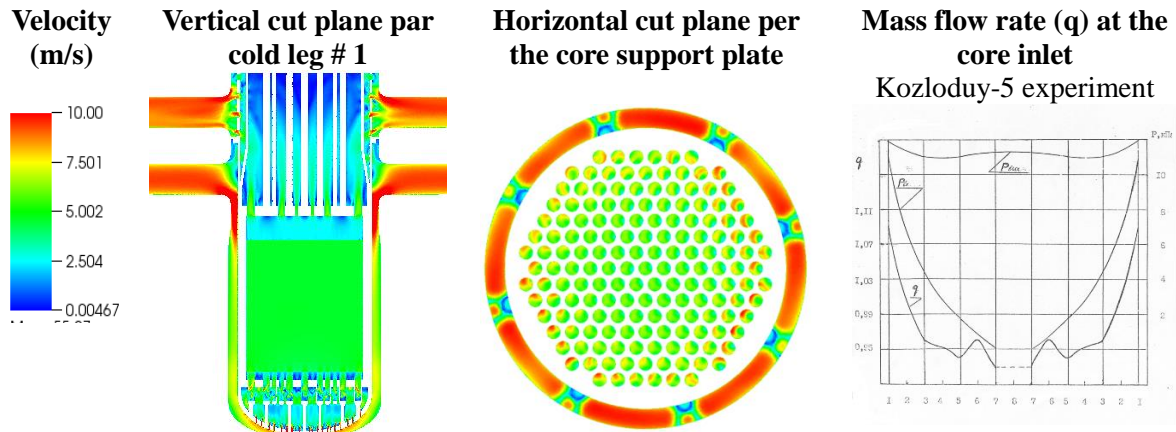


Fig. 15 Velocity distribution at the core inlet and in the RPV

## 8. CONCLUSIONS

A steam generator separation test performed in the framework of a licensing experiment in the Kozloduy-6 VVER-1000 reactor was analyzed with CFD. The whole RPV with all important internals was meshed explicitly; only the core region was modelled by a porous media approach. Grids with up to 400 million tetrahedrons and 800 million velocity control volumes have been created. The numerical approach was first validated by three single effect tests which have been selected due to a previously

performed PIRT. The calculation shows a good agreement to the measured temperature distribution at the core outlet as well as loop to assembly and loop to loop mixing coefficients. The calculated velocity at the core inlet is also in good accordance to measurements. Doubts arise concerning the experimental procedure to estimate the core inlet temperature; the turbulent mixing in the core region has been neglected.

## 9. ACKNOWLEDGMENTS

This work was granted access to the HPC resources of CINES under the allocation x20162a7571 made by GENCI.

## REFERENCES

- 1 NEA/NSC/DOC(2010)10, “VVER-1000 Coolant Transient Benchmark Phase 2 (V1000CT-2) Summary Results of Exercise 1 on Vessel Mixing Simulation”, OECD/NEA Report.
- 2 NEA/NSC/DOC(2007)22, “VVER-1000 Coolant Transient Benchmark Phase 2 (V1000CT-2) Final Specifications of the VVER-1000 Vessel Mixing Problem”, OECD/NEA Report.
- 3 U. Bieder, et al., “Simulation of mixing effects in a VVER-1000 reactor”, *Nuclear Eng. Design*, 237(15-17), pp.1718-1728 (2007).
- 4 M. Böttcher, “Detailed CFX-5 study of the coolant mixing within the reactor pressure vessel of a VVER-1000 reactor during a non-symmetrical heat-up test”, *Nuclear Eng. Design*, **238**(3), pp.445-452 (2008).
- 5 H. Farajollahi, “CFD-Calculation of Fluid Flow in a Pressurized Water Reactor”, *Journal of Sciences*, Islamic Republic of Iran 19(3): 273-281 (2008)
- 6 C.V. Hirt, Nichols, B.D., Romero, N.C., 1975. “SOLA—a numerical solution algorithm for transient flow”, Los Alamos National Lab., Report LA-5852.
- 7 J.-L. Guermond, et al., “On the Stability and Convergence of Projection Methods Based on Pressure Poisson Equation”, *Int. J. Numer. Meth. Fluids* 26: 1039–1053 (1998)
- 8 J. Mahaffy, “Best Practice Guidelines for the Use of CFD in Nuclear Safety Applications”, NEA/CSNI/R(2007)5.
- 9 B. Gaudron, et al, “Using the PIRT to represent application and validation domains for CFD studies”, *Proceedings of ICONE-23*, 5/17-21/2015, Chiba, Japan.
- 10 C. Terrier, “Improving confidence in CFD results for nuclear safety demonstration – Example of heterogeneous inherent boron dilution”, *Proceedings of ICONE-23*, 5/17-21/2015, Chiba, Japan.
- 11 I.E. Idelchik, *HANDBOOK OF HYDRAULIC RESISTANCE*, 4th edition, 2008
- 12 U. Bieder, et al., “Analysis of the Natural Convection Flow in the Upper Plenum of the MONJU Reactor with Trio\_U”, *Science and Technology of Nuclear Installations*, 5/2013.
- 13 Trio\_U, 2006. <http://www-trio-u.cea.fr/>